Atmospheric
Chemistry
and Physics
Discussions

Open Access

EGU

1 **Assessment of dicarbonyl contributions to secondary organic aerosols over China**

2 **using RAMS-CMAQ**

3 Jialin Li [1], Meigen Zhang [1, 2, 3, *], Guiqian Tang [1], Yele Sun [1, 2, 3], Fangkun Wu [1],

4 Yongfu Xu [1, 3]

5

6 [1]State Key Laboratory of Atmospheric Boundary Layer Physics and Atmospheric Chemistry,

7 Institute of Atmospheric Physics, Chinese Academy of Sciences, Beijing 100029, China

8 [2]Center for Excellence in Regional Atmospheric Environment, Institute of Urban Environment,

9 Chinese Academy of Sciences, Xiamen 361021, China

10 [3]University of Chinese Academy of Sciences, Beijing 100049, China

11

12 **Abstract**

13 The concentration of secondary organic aerosol (SOA) is underestimated by one to two orders of

14 magnitude in current model studies. Recent research suggests that the aqueous irreversible uptake

15 of dicarbonyls contributes to the production of SOA, although few models have included this

16 pathway. Glyoxal, an important representative component of dicarbonyls in models, is significantly

17 underestimated. We therefore incorporated the aqueous irreversible uptake of dicarbonyls into the

18 regional air quality modeling system RAMS-CMAQ (the Regional Atmospheric Modeling System-

19 Community Multiscale Air Quality) to evaluate the contribution of dicardonyls to SOA, and we then

20 assess the impact of the underestimation of glyoxal on the production of SOA in China during two

21 time periods: June 3 to July 11, 2014 (episode 1) and October 14 to November 14, 2014 (episode 2).

22 When the aqueous irreversible uptake process was added, the modeled mean concentration of SOA

23 in episode 1 increased by 1.57 μg/m^3, which explains 15.0% of the unaccounted source of SOA. By

24 contrast, the increase in the concentration of SOA in episode 2 was small as a result of the lower

25 liquid water content and the lower amount of dicarbonyls produced from biogenic precursors in the

26 fall. On this basis, when the glyoxal simulation was improved, the modeled mean dicarbonyl-

27 derived SOA (AORGCJ) increased by a factor of 2 in both episodes. AORGCJ in episode 1

28 contributed, on average, 39.0% of the total concentration of SOA and the increase in this

29 contribution represented 26.7% of the unaccounted concentration of SOA, whereas the mean

30 AORGCJ in episode 2 accounted for 18.5% of total concentration of SOA. Based on the results for

31 episode 1, the mean AORGCJ in summer over China was generally higher in the east than in the

Atmospheric
Chemistry
and Physics
Discussions

32   west, with the highest value (5–10 µg/m^3) in the areas between the lower reaches of the Yellow and

33   Yangtze rivers and in the Sichuan Basin. The contribution of AORGCJ to the concentration of SOA

34   varied from 10 to 90% throughout China, with the highest contributions (70–90%) in the coastal

35   regions and offshore along the East China Sea to the South China Sea and in the southwestern

36   regions.

37   **Keywords:** secondary organic aerosol, aqueous irreversible uptake, glyoxal, China, RAMS-CAMQ

38

39   **1. Introduction**

40   The fine particle fraction of aerosols (PM$_{2.5}$, i.e., particulate matter with an aerodynamic diameter

41   ≤ 2.5 µm) not only absorbs and scatters sunlight in the atmosphere, resulting in a reduction in

42   visibility and effects on the global climate (IPCC, 2007), but also has adverse effects on human

43   health (Harrison and Yin, 2000;Poschl, 2005). Organic aerosol (OA) is a major component of fine

44   particulate matter globally (Murphy et al., 2006;Zhang et al., 2007), typically making up 20–90%

45   of the fine particle fraction (Kanakidou et al., 2005;Roberts et al., 2001;Zhang et al., 2007),

46   suggesting that it has a significant effect on the characteristics and properties of fine particulate

47   matter. Organic aerosols are formed from both primary (direct emissions) and secondary sources.

48   Secondary organic aerosols (SOAs) are formed from precursors of volatile organic compounds

49   (VOCs), which can be either natural or anthropogenic. However, the underestimation of organic

50   aerosol has become a major issue in almost all current atmospheric models due to the incomplete

51   representation of SOA (Goldstein and Galbally, 2007;Heald et al., 2005;Morris et al., 2006;Morris

52   et al., 2005;Yu et al., 2008).

53   It has been reported that the concentration of SOA in current models is underestimated by one to

54   two orders of magnitude (de Gouw et al., 2005;Volkamer et al., 2006). These results have motivated

55   researchers to investigate why these models are predicting SOA concentrations so poorly.

56   Traditionally, improvements in models have mainly concentrated on the gas-phase and derived

57   heterogeneous formation processes, such as the formation of SOA from aromatic compounds under

58   low- and high-NO$_x$ conditions (Ng et al., 2007), the production of SOA from the oxidation of

59   isoprene and its subsequent growth through acid catalysis (Kroll et al., 2005, 2006;Surratt et al.,

60   2007), the use of volatile bias set method to depict the formation of SOA instead of the two-product

61   model (Han et al., 2016;Lane et al., 2008;Lin et al., 2016;Murphy and Pandis, 2009), and the

Atmospheric
Chemistry
and Physics
Discussions

62   formation of SOA through the uptake of isoprene epoxides on the surface of aerosols (Hu et al.,

63   2017;Ying et al., 2015). In spite of these researches, biases still exist between the simulations and

64   observations.

65   Many studies have suggested that glyoxal and methylglyoxal can form SOAs through chemical

66   reactions in cloud or fog water (e.g.Carlton et al., 2006;Ervens et al., 2004;Lim and Ziemann,

67   2005;Loeffler et al., 2006;Warneck, 2003), or by irreversible uptake on the surface of cloud droplets

68   and aqueous aerosols (e.g. Corrigan et al., 2008;Galloway et al., 2009;Liggio et al., 2005), which is

69   probably a significant source of SOA (Curry et al., 2018;Ervens et al., 2014). A few studies

70   (e.g.Carlton et al., 2010;Carlton et al., 2008;Fu et al., 2009;Li et al., 2013) have incorporated

71   aqueous formation pathways into atmospheric models. These studies have shown that chemical

72   reactions in cloud or fog water make negligible contribution to near-surface SOA relative to

73   irreversible uptake on the surface of cloud droplets and aqueous aerosols, and that the aqueous

74   formation of SOA cannot completely explain the gaps between the observations and simulations.

75   There are still considerable uncertainties in our knowledge of the formation of SOA.

76   A series of studies (Fu et al., 2008;Liu et al., 2012;Myriokefalitakis et al., 2008;Li et al., 2018)

77   has shown that there is a substantial underestimation in the modeled vertical column densities

78   (VCDs) of glyoxal, but few studies have considered the impact of this underestimation on

79   simulations of SOA concentrations. Xu et al. (2017) and Ervens et al. (2011) showed that the

80   aqueous formation of SOA depends on the liquid water content (LWC), which varies between

81   seasons. Previous studies, such as those of Fu et al. (2009) and Li et al. (2013), have only considered

82   the contribution from SOA derived from the aqueous irreversible uptake of dicarbonyls (pathway

83   M) in the summer period or over evergreen areas. In this study, we not only incorporated pathway

84   M into the RAMS-CMAQ (the Regional Atmospheric Modeling System-Community Multiscale

85   Air Quality) modeling system to evaluate the corresponding contribution of dicarbonyls to SOA,

86   but also improved the simulation of glyoxal concentrations by investigating the reasons for its

87   underestimation and assessing its impacts on the concentration of SOA during two episodes in the

88   summer and fall.

89

90   **2. Model and data**

91   **2.1 Base model description**

92   Li et al. (2017a) used the RAMS-CMAQ modeling system to investigate the effects of

93   underestimated aromatic VOC emissions and yields of SOAs from different gas precursors on the

94   concentration of SOAs. Similarly, we used Version 4.7.1 of the CMAQ, which is coupled with the

95   gas-phase photochemical mechanism SAPRC99 (1999 Statewide Air Pollutant Research Center

96   (Carter, 2000) and Version 5 of the aerosol module (AERO5) (Byun and Schere, 2006;Foley et al.,

97   2010). There are three major formation pathways for SOAs in this version, which is based on the

98   two-product approach. The first pathway is the equilibrium partition of semi-volatile products

99   formed from the oxidation of seven VOC precursors: long-chain alkanes, benzene (BNZ), high-

100   yield aromatics (mainly toluene, ARO1), low-yield aromatics (mainly xylene, ARO2), isoprene

101   (ISOP), monoterpene (TRP) and sesquiterpenes (SESQ). The second pathway is the oligomerization

102   of semi-volatile SOAs formed through the first pathway (Kalberer et al., 2004), namely aging

103   process. The third pathway is the formation of SOA via the in-cloud oxidation of glyoxal (GLY) and

104   methylglyoxal (MGLY) (Carlton et al., 2008), both of which represent dicarbonyls in the model.

105   The details of these formation pathways are given in Carlton et al. (2010).

106   The meteorological fields used to drive CMAQ are obtained from RAMS, which has been

107   described in detail by Cotton et al. (2003). The National Centers for Environmental Prediction

108   reanalysis datasets are served as the initial meteorological fields input into RAMS. The boundary

109   conditions used for the RAMS computations include the weekly average sea surface temperature

110   and the monthly measured snow cover. The final modeled results are output through the four-

111   dimensional data assimilation mode using nudging analysis.

112   The emission sources are derived from several different inventories. Anthropogenic emissions

113   (Li et al., 2017b)—including SO_2, NO_x, CO, black carbon, non-methane VOCs, organic carbon,

114   NH_3 and other particulate matter—are obtained from the monthly emissions inventory of 2012.

115   There are five emission sectors (the power, industrial, residential, transportation and agricultural

116   sectors) in the inventory with a spatial resolution of $0.25° \times 0.25°$ (see www.meicmodel.org). The

117   Model of Emissions of Gases and Aerosols from Nature (MEGAN) (Guenther et al., 2012) provides

118   the biogenic emissions. The emissions from open biomass burning are derived from the Global Fire

119   Emissions Database, Version 4 (Randerson et al., 2015), whereas the information of monthly

120   lightning NO_x is obtained from the Global Emissions Inventory Activity with a spatial resolution of

121    $1° \times 1°$ (Benkovitz et al., 1996). The emissions of NO_x from the soil are derived from the Regional

Atmospheric
Chemistry
and Physics
Discussions

122   Emission inventory in ASia, Version 2.1, with a spatial resolution of 0.25° × 0.25° (Kurokawa et al.,

123   2013). The online dust and sea salt emissions are calculated using the empirical model developed

124   by Han et al. (2004) and the scheme of Gong (2003), respectively. The calculation of the model

125   boundary conditions is supported by the Model of Ozone and Related Tracers, Version 4 (MOZART-

126   4) (Emmons et al., 2010).

127   The model domain is divided into 105 × 86 grid cells with the center located at (35° N, 110° E)

128   (Fig. 1). The map projection is rotated polar-stereographic with a horizontal resolution of 64 km.

129   The vertical simulation region is unequally spaced from the ground surface to ~23 km. There are 25

130   layers in the σ_z coordinate system in RAMS, with nine layers located in the lowest 2 km to resolve

131   the planetary boundary layer. The vertical dimension of CMAQ is divided into 15 layers, with the

132   lowest seven layers the same as those in RAMS. We focused on the area outlined by the blue box in

133   Fig. 1.

134

135   **2.2 Adding the aqueous irreversible uptake process**

136   Pathway M was implemented in the cloud module of CMAQ following the standard reaction

137   probability formulation of Jacob (2000). In this formulation, the first-order rate constant k for the

138   chemical loss of a gas-phase species to the aerosols or cloud droplets through molecular diffusion

139   and free collision is given by

140   $$k = \left(\frac{a}{D_g} + \frac{4}{v\gamma} \right)^{-1} A \tag{1}$$

141   where D_g is the gas-phase molecular diffusion coefficient, a is the radius of the aerosol particle or

142   cloud droplet, v is the mean molecular speed, γ is the reaction uptake coefficient when a collision

143   occurs between a gas-phase molecule and the aqueous surface, and A is the aqueous particle surface

144   area per unit volume of air.

145   In a similar manner to Fu et al. (2008), diffusion limitation ($D_g A/a$) is applied in the model to

146   account for the uptake of gas by cloud droplets. As we are mainly concerned with continental regions,

147   the cloud droplet surface area is calculated from the LWC in the cloudy fraction by assuming an

148   effective droplet radius of 6 μm (Li et al., 2013). D_g is chosen as the typical tropospheric value given

149   by Jacob (2000). The collision limitation ($v\gamma A/4$) is then used to compute the uptake of gas by

150   aqueous aerosols as reported by Ying et al. (2015). The value of $\gamma = 2.9 \times 10^{-3}$ adopted here for both

Atmospheric
Chemistry
and Physics
Discussions

151   glyoxal and methylglyoxal is from Liggio et al. (2005).

152

153   **2.3 Observational data**

154   To assess the contribution of dicarbonyl species to the concentration of SOA, we used the observed

155   concentration of SOA in Beijing during the summer and fall of 2014 measured by Xu et al. (2017)

156   with an Aerodyne high-resolution time-of-flight aerosol mass spectrometer. Samples were taken

157   from June 3 to July 11, 2014 and October 14 to November 14, 2014 at the Institute of Atmospheric

158   Physics. More detailed information about the data has been reported by Xu et al. (2017). The

159   simulation periods are from May 22 to July 11 and from October 1 to November 14, with the first

160   12 days as the spin-up time. To evaluate the reasonability in simulating the formation processes of

161   SOAs in the aqueous phase, the corresponding cloud water path (CWP) data measured by the

162   MODerate Resolution Imaging Spectroradiometer (MODIS) was also obtained from the website

163   http://ladsweb.modaps.eosdis.nasa.gov/api/v1/productPage/product=MYDATML2.

164   Liu et al. (2012) and Li et al. (2018) have suggested that the underestimation of glyoxal

165   concentrations in simulations is related to the underpredicted emission of aromatic compounds and

166   the molar yields of glyoxal from the precursors. Therefore the biases in the emission of aromatic

167   compounds needs to be evaluated through a comparison of the observed and simulated

168   concentrations of aromatic compounds. The observed data were collected at 14:00 local standard

169   time every Thursday by gas chromatography–mass spectrometer at Beijing, Xinglong and Yucheng

170   (Fig. 1). Sun et al. (2016) and Wu et al. (2016) have presented the detailed information.

171   To evaluate the performance of our model, we also compared the simulated $PM_{2.5}$ concentrations

172   and several meteorological factors with the results measured over 12 stations (Fig. 1) during the two

173   episodes. The observed meteorological data were derived from the Meteorological Information

174   Comprehensive Analysis and Process System (MICAPS) dataset, whereas the Chinese National

175   Environmental Monitoring Center provided the measured concentrations of $PM_{2.5}$.

176

177   **3. Results and discussions**

178   **3.1 Model evaluation**

179   Table 1 shows statistical results of the meteorological parameters (i.e. temperature, relative humidity,

180   wind speed and wind direction) and $PM_{2.5}$ concentrations in the two analyzed episodes, where: *N* is

Atmospheric
Chemistry
and Physics
Discussions

Open Access

181   the total number of samples; IOA is the index of agreement, which can synthetically reflect the

182   combination of the modeled value and variable tendency being good or bad (Willmott, 1981); C_{mod}

183   and C_{obs} are the average values of modeled and observed results, respectively; MB and FB are the

184   mean and fractional bias, respectively; RMSE and FE are the root-mean-square and fractional error,

185   respectively; and R is the correlation coefficient between the observed and simulated results. The

186   calculations of these statistical parameters can be found in Juda-Rezler et al. (2012). $P_{22.5°}$ and $P_{45°}$

187   represent the proportions of compared results that the absolute biases between the simulated and

188   measured wind directions are within 22.5° and 45°, respectively (Li et al., 2017a).

189   There are inevitably some biases in the simulated meteorological parameters relative to the

190   observations due to the limited model resolution and system errors. Nevertheless, the model

191   reproduces the magnitude and variation trend of the temperature and relative humidity fairly well

192   (Figs. S1 and S2), with IOAs for temperature of 0.91 and 0.95 in the two episodes and IOAs of 0.91

193   and 0.88 for the relative humidity, comparable with the results of Li et al. (2012) and Wang et al.

194   (2014). The mean biases of temperature (–0.83°C, –0.68°C) and relative humidity (1.53%, –0.05%)

195   are small in the two episodes. The RMSEs of temperature and relative humidity are comparable

196   with the results of Gao et al. (2016) and Zhang et al. (2012), implying a reasonable performance of

197   the simulation. Although the capture of the variable tendency of wind speed (Fig. S3) by the model

198   is rather poor, the small values for the mean bias (–0.40 and –0.22 m/s) and the high IOAs (0.61 and

199   0.69) indicate a better performance than that reported by Feng et al. (2016) and Wang et al. (2014)

200   in simulating the wind speed. The RMSE of wind speed shows that the simulated results achieve

201   the criteria for a good performance (|RMSE| ≤ 2 m/s) given by Emery et al. (2001). For the wind

202   direction (Fig. S4), $P_{22.5°}$ and $P_{45°}$ are 32.12 and 54.52% in episode 1 and 34.01 and 57.41% in

203   episode 2, indicating the reasonable simulation of wind direction. Therefore the model provides a

204   reasonable meteorological field for the subsequent simulations.

205   The modeled $PM_{2.5}$ concentrations are generally higher than the observed values in the two

206   episodes over the 12 stations (Fig. S5). Except for the limited resolution of the model, the

207   uncertainties of the emission inventory and the effects of the background transport may also

208   contribute to the overestimation. However, the correlation coefficients of $PM_{2.5}$ are 0.50 and 0.56 in

209   the two episodes, respectively, and the IOAs are 0.64 and 0.70 in the two episodes, respectively,

210   indicating good capture of the variable tendency and magnitude by the model. Both the fractional

Atmospheric
Chemistry
and Physics
Discussions

211   error and the fractional bias for PM$_{2.5}$ in the two episodes fulfill the performance criteria (FE $\leqslant$

212   75%, |FB| $\leqslant$ 60%) given by Boylan and Russell (2006), implying a good performance in

213   simulating PM$_{2.5}$. These results show that the model gives a reasonable simulation of the chemical

214   species.

215   As described in Section 2.2, pathway M is related to the cloud water content. Thus the modeled

216   and satellite-observed mean CWP were compared during the two analyzed episodes to evaluate the

217   reasonability of the simulation results. Fig. 2a and 2b show that in episode 1, during one summer

218   period, the highest observed CWP (400–500 g/m^2) mainly appears over the Yellow Sea and Bohai

219   Sea and in parts of southeastern and southern China, whereas the observed second highest values

220   (200–300 g/m^2) are concentrated in from the Qinghai–Tibetan Plateau to the North China Plain

221   along the Yellow River Basin. The modeled high CWP (100–400 g/m^2) appears in the same regions

222   as in the observational dataset. In episode 2, during one fall period (Fig. 2c and 2d), the observed

223   highest (300–500 g/m^2) and second highest (200–300 g/m^2) CWP values are mainly concentrated in

224   the Hetao area and the regions including the northeastern China and Inner Mongolia, respectively.

225   The modeled values (50–150 g/m^2) are also high over these regions.

226   Overall, there are obvious biases in the numerical values between the observed and simulated

227   CWP. This is a result of the large uncertainties in both the model simulations and the satellite

228   retrievals of clouds, which lead to uncertainties in the simulations of the concentrations of SOAs.

229   However, the mean distribution patterns of the simulated CWP during the two episodes are similar

230   to the observational results, indicating few impacts on the simulated distribution of SOA. Both the

231   simulated and observed CWP in episode 1 are higher than in episode 2, also implying differences in

232   the simulation of SOA between the two episodes.

233

234   **3.2 Model results and analyses**

235   As described in Section 2.3 and with reference to previous research, the underestimation of glyoxal

236   concentrations may result from the underprediction of the emissions of aromatic compounds and

237   the molar yields of glyoxal from the precursor molecules. It is therefore necessary to evaluate the

238   emissions of aromatic compounds during the analyzed episodes before designing and implementing

239   the model case studies. For this purpose, comparisons were made between the simulated and

240   observed concentrations of aromatic compounds in a similar manner to the work of Zhang and Ying

Atmospheric
Chemistry
and Physics
Discussions

241   (2011).

242   Fig. 3 presents the ratio of the observed to predicted (O/P ratio) concentrations of aromatic

243   compounds for the original emissions (Fig. 3a and 3c) and a three-fold increase in the emissions of

244   aromatic compounds (Fig. 3b and 3d) during the two episodes. Fig. 3a shows that there are biases

245   between the observed and simulated concentrations of aromatic compounds in episode 1 at the

246   original emission rates of the aromatic compounds. The O/P ratios are more concentrated for ARO1

247   than for ARO2, with both the mean and median O/P values being close to 2. The range of O/P values

248   is large for ARO2 and there is an order of magnitude difference between the lowest and highest

249   ratios. Both the mean and median O/P ratios of ARO2 are about 20. These results show that there

250   are underestimations in the emissions of ARO1 and ARO2. In view of the limitations of the amount

251   of observed data and the nonlinear relationship between emissions and the concentrations (Li et al.,

252   2018), the underestimation in the emission rates has been conservatively estimated to be a factor of

253   three. As a result, when the emission rates of aromatic compounds are increased (Fig. 3b), the ratios

254   of ARO1 and ARO2 in episode 1 are more concentrated, especially ARO2. The mean and median

255   ratios of ARO1 are both around 1, whereas the two ratios for ARO2 decrease from 20 to 6. The

256   results for episode 2 are similar to those in episode 1. Fig. 3c shows that the original O/P ratio of

257   ARO1 varies between 1 and 3.5, with a mean value close to 2, whereas the ratio of ARO2 ranges

258   from 1 to 5, with a mean ratio of about 4, both of which indicate unaccounted emissions of aromatic

259   compounds. Fig. 3d shows a clear decrease in the biases of the observed and simulated

260   concentrations of aromatic compounds. The O/P ratios of ARO1 and ARO2 are concentrated and

261   vary between 1 and 2, with a mean ratio close to 1. However, it is difficult to determine whether the

262   factor of 3 is the actual underestimation in the emission of aromatic compounds as a result of its

263   dependence on space and time. For convenience, a factor of 3 is chosen here as a uniform scale with

264   which to assess the unaccounted emissions of aromatic compounds.

265   Three sensitivity simulation case studies were designed based on these results. Case 0 is the base

266   example and was performed with the standard model. Case 1 was run with the modified model

267   incorporating pathway M. By combining our results with those of Li et al. (2018), case 2 was

268   designed to take the effects of the underestimations of glyoxal concentrations into considerations

269   (i.e. a three-fold increase in the emissions of aromatic compounds and a five-fold increase in the

270   molar yield of glyoxal from isoprene) based on the results of case 1.

Atmospheric
Chemistry
and Physics
Discussions

271   Fig. 4 compares the hourly concentrations of the simulated and observed SOAs during the two

272   analyzed episodes; the corresponding statistical parameters are listed in Table 2. The concentrations

273   of SOAs are measured from PM_1. The observed $PM_1/PM_{2.5}$ ratio of 0.77 (Xu et al., 2015) was used

274   to convert the observed concentrations for comparison with the simulated results for $PM_{2.5}$.

275   In case 0, the SOA concentrations in episode 1(Fig. 4a) are significantly underestimated by an

276   average factor of 5.7, with the differences being as high as a multiple of ≥ 60. As a result of the

277   impacts of uncertainties in the meteorological fields and emissions, the variation trend of the

278   concentration of SOA was not well captured by the model ($R = 0.21$). Similarly, although the

279   variation of SOA was reproduced well in episode 2 ($R = 0.83$) (Fig. 4b), the concentration of SOA

280   was still underpredicted by an order of magnitude. The biases between the observed and simulated

281   concentrations of SOAs decreased in case 1 when pathway M was added to the model, especially in

282   episode 1. Fig. 4c shows that the mean concentration of SOA in case 1 increased by 1.57 μg/m^3

283   during episode 1, explaining 15.0% of the unaccounted sources of SOAs. The decreased mean bias

284   and RMSE and the slightly increased IOA also indicate the more reasonable descriptions of the

285   formations of SOAs. In episode 2, the SOA formed through pathway M contributed less to the total

286   concentration of SOA (Fig. 4d). The mean SOA concentration during episode 2 reached 1.31 μg/m^3,

287   an increase of only 0.26 μg/m^3. The other statistical parameters showed little change, indicating the

288   small contribution of dicarbonyls through pathway M to the concentration of SOA in this episode.

289   The larger contribution of dicarbonyls from pathway M to the concentration of SOA in episode 1 is

290   attributed to the higher LWC and the larger amount of dicarbonyls produced from biogenic

291   precursors in the summer than in the fall. When the impact of the underestimation of glyoxal on the

292   concentration of SOA is taken into consideration, the concentration of SOA clearly increases in case

293   2. Fig. 4e and 4f show that the mean concentration of SOA in episode 1 is significantly improved

294   by a factor of 2.3, whereas the increase in episode 2 is a factor of 1.8. The statistical parameters (e.g.

295   IOA, R and RMSE) also show the better performance of case 2, indicating a more realistic and

296   reasonable representation of the formation of SOA. Aromatic compounds are not only the precursors

297   of glyoxal, but are also a precursor of SOA in the gas phase. A compositional analysis is therefore

298   required to evaluate the individual contributions from dicarbonyls in case 2.

299   Fig. 5 shows the mean contributions from different sources of SOAs in the three sensitivity case

300   studies during the two analyzed episodes. AORGCJ, dicarbonyl-derived SOAs, contributes little in

Atmospheric
Chemistry
and Physics
Discussions

301   case 0 during the two episodes. The mean contribution of AORGCJ to the total concentration of

302   SOAs in episode 1 is 2.39%, larger than in episode 2 (0.89%). As a result of the greater amount of

303   emissions from biogenic sources in summer, SOAs formed from biogenic precursors

304   (AISOP+ATRP+ASQT) contribute more (26.3%) in episode 1 than that in episode 2 (13.5%),

305   whereas the contributions from anthropogenic precursors (AALK+ATOL+AXYL+ABNZ) are

306   comparable between the two episodes. When pathway M is included in the model, the contribution

307   from AORGCJ to SOA in case 1 clearly increases and reaches 37.1% in episode 1 and 19.3% in

308   episode 2. The contribution from AORGCJ in episode 1 is higher than the contributions from

309   anthropogenic (26.9%) and biogenic (16.6%) gas precursors, indicating the significant contributions

310   from dicarbonyls through pathway M to the formations of SOAs in summer. When the impact of

311   the underestimation of glyoxal is taken into consideration in case 2, the mean concentration of

312   AORGCJ in both episodes increases by nearly a factor of 2 relative to case 1. In episode 1, AORGCJ

313   (2.85 µg/m^3) accounts for 39.0% of the total SOA, exceeding the sum of the contributions from

314   ARO1 (ATOL) and ARO2 (AXYL) (26.0%), and indicating the dominant contribution of aqueous-

315   phase process to the concentration of SOA in summer. The increase in AORGCJ compensates for

316   about 26.7% of the unaccounted sources of SOAs. In episode 2, AORGCJ (0.56 µg/m^3) contributes

317   18.5% to the total concentration of SOA, which is much less than the sum of ATOL and AXYL

318   (38.3%), implying the dominant contributions of aromatic compounds to the concentrations of

319   SOAs. The different contributions of AORGCJ in case 2 during the two episodes can be attributed

320   to the different LWC and different amount of dicarbonyls produced from biogenic precursors.

321   It is clear that the biases between the observed and simulated concentrations of SOAs decrease

322   when the contributions of unaccounted dicarbonyls to the concentrations of SOAs are considered,

323   especially in summer. However, the sources of unaccounted SOAs cannot be explained completely.

324   As a result of uncertainties in the description of known SOA formation processes and missing

325   pathways that have not been included in the model—for example, there are many uncertainties in

326   glyoxal simulations (Li et al. (2018)). There are also many uncertainties in incorporating pathway

327   M into the model, such as the effective radius of cloud droplets (the model only considers the

328   empirical value over continental regions), the diffusion coefficient (which does not consider the

329   impacts of temperature, molecular weight and air density), the reaction uptake coefficient (updated

330   values over disparate land surfaces are discussed in Curry et al. (2018)) and the liquid water content

Atmospheric
Chemistry
and Physics
Discussions

Open Access

EGU

331   in clouds (the most uncertain parameter in Fig. 2). This study considers the formation of SOA in

332   clouds through pathway M, but neglects processes occurring on the surface of fog droplets or

333   aqueous aerosols near the ground, which may be important sources of SOAs in fall and winter. Other

334   pathways for the formations of SOAs, such as the uptake of isoprene epoxides on the surface of

335   aerosols (Lal et al., 2012;Lin et al., 2013), the aging mechanism of semi-volatile primary organic

336   aerosols (Shrivastava et al., 2008) and the oxidation of primary semi- and intermediate VOCs, have

337   not been considered in this model.

338   To distinguish the contribution of dicarbonyls to the concentration of SOA over China, the

339   distributions of dicarbonyl-derived SOAs and their contributions to SOAs (AORGCJ/SOA) over

340   China in cases 0 and 2 were analyzed. The contributions from AORGCJ were not clear in episode

341   2, thus only the results for episode 1 are here.

342   Fig. 6a and 6b show the mean concentration of AORGCJ in cases 0 and 2, respectively, during

343   episode 1. For the base case, the concentration of AORGCJ over China is ≤ 0.2 μg/m^3. The

344   concentration of AORGCJ is higher (0.1–0.2 μg/m^3) in the areas between the lower reaches of the

345   Yellow and Yangtze rivers and in the Sichuan Basin, probably due to the higher LWC and a greater

346   number of sources of dicarbonyls over these areas, as discussed in Section 3.1 and by Li et al. (2018).

347   The concentration of AORGCJ is clearly improved in case 2, when pathway M is added and the

348   impact of the underestimation of glyoxal is considered. Overall, the concentration of AORGCJ is

349   higher in eastern China than in the west. The concentrations of AORGCJ vary from 2 to 5 μg/m^3

350   over central and eastern China, with the highest value (5–10 μg/m^3) concentrated in the same areas

351   as in case 0. The concentration of AORGCJ in western China is ≤ 1 μg/m^3, with the lowest value ($\leq$

352   0.1 μg/m^3) in the northeast, probably because there are few sources of dicarbonyls here.

353   Fig. 6c and 6d show the spatial distribution of the mean AORGCJ/SOA in cases 0 and 2 during

354   episode 1, respectively. Fig. 6c shows that the AORGCJ fraction over China is $\leq 10\%$, except in

355   Yunnan Province and some parts of the South China Sea, where AORGCJ/SOA reaches 10–20%.

356   When the contributions of dicarbonyls from pathway M and improved glyoxal to SOA are

357   considered, there is a large increase in AORGCJ/SOA over these regions. Fig. 6d shows that the

358   contribution of AORGCJ to SOA varies from 10 to 90% throughout China. In central and eastern

359   areas, the fraction of AORGCJ is generally in the range of 40–60% and up to 70–90% in the coastal

360   regions and offshore from the East China Sea to the South China Sea. The fraction of AORGCJ in

Atmospheric
Chemistry
and Physics
Discussions

361   the west is relatively low and usually ≤ 40%. However, the contribution of AORGCJ to SOA is up

362   to 80% in southwestern regions (e.g. Yunnan Province and parts of Sichuan Province).

363   **4. Conclusions**

364   The RAMS-CMAQ modeling system was used to assess the contributions of dicarbonyls from the

365   aqueous irreversible uptake process and unaccounted sources of glyoxal to the concentrations of

366   SOAs during two episodes from June 3 to July 11, 2014 and October 14 to November 14, 2014.

367   Comparisons between the observed and simulated concentrations of SOAs from three sensitivity

368   groups showed different improvements in the SOA simulations with the inclusion of pathway M

369   and consideration of the underestimation of glyoxal in the two episodes. Due to the high LWC and

370   large amount of dicarbonyls produced from biogenic precursors in summer, the contributions of

371   dicarbonyls were greater in episode 1 than in episode 2. When pathway M was added in case 1, the

372   modeled mean concentration of SOA in episode 1 increased by 1.57 $\mu g/m^3$, explaining about 15.0%

373   of the unaccounted SOA sources, whereas there was only a 0.26 $\mu g/m^3$ increase in the mean result

374   during episode 2. When the impacts of glyoxal underestimation were taken into consideration in

375   case 2, the modeled mean AORGCJ in episode 1 was improved by a factor of 2 and contributed

376   39.0% of the total concentration of SOA. The increase due to AORGCJ is equivalent to 26.7% of

377   the unaccounted source of SOA. Whereas the mean concentration of AOGRCJ in episode 2 was

378   only 0.56 $\mu g/m^3$ and accounted for 18.5% of total concentration of SOA. Although the contributions

379   of dicarbonyls to SOAs are different in the two episodes, the simulated SOA results are both

380   improved and close to the observations, indicating a more realistic description of aqueous formation

381   of SOA.

382   The mean AORGCJ in case 2 during episode 1 was clearly improved over China relative to case

383   0 and was generally higher in the east than in the west. The highest value (5–10 $\mu g/m^3$) was seen in

384   the areas between the lower reaches of the Yellow and Yangtze rivers and in the Sichuan Basin, as

385   a result of the combination of a higher liquid water content and the greater number of dicarbonyl

386   sources in these areas. As a result, the contribution of AORGCJ to the concentration of SOA in

387   episode 1 was also improved in case 2. The fraction varied from 10 to 90% throughout China, with

388   the highest contribution (70–90%) in the coastal regions or offshore along the East China Sea to the

389   South China Sea in addition to the southwestern regions (e.g. Yunnan Province and parts of Sichuan

390   Province).

Atmospheric
Chemistry
and Physics
Discussions

391   It is clear that the contributions of dicarbonyls from pathway M and the unaccounted sources of

392   glyoxal make a significant contribution to the concentration of SOA, especially in summer. However,

393   there are still many uncertainties in the depictions of aqueous irreversible uptake processes and

394   sources of glyoxal. More work is needed on the parameters used in pathway M (e.g. the effective

395   radius of cloud droplets, the diffusion coefficient, and the reaction uptake coefficient), and to

396   improve the accuracy of the modeled liquid water content in clouds.

397

409

410   **References**

411   Benkovitz, C. M., Scholtz, M. T., Pacyna, J., Tarrason, L., Dignon, J., Voldner, E. C., Spiro, P. A., Logan, J. A., and

412   Graedel, T. E.: Global gridded inventories of anthropogenic emissions of sulfur and nitrogen, J. Geophys. Res.-

413   Atmos., 101, 29239-29253, 10.1029/96jd00126, 1996.

414   Boylan, J. W., and Russell, A. G.: PM and light extinction model performance metrics, goals, and criteria for three-

415   dimensional air quality models, Atmos. Environ., 40, 4946-4959, 10.1016/j.atmosenv.2005.09.087, 2006.

416   Byun, D., and Schere, K. L.: Review of the governing equations, computational algorithms, and other components

417   of the models-3 Community Multiscale Air Quality (CMAQ) modeling system, Applied Mechanics Reviews, 59,

418   51-77, 10.1115/1.2128636, 2006.

419   Carlton, A. G., Turpin, B. J., Lim, H. J., Altieri, K. E., and Seitzinger, S.: Link between isoprene and secondary

420   organic aerosol (SOA): Pyruvic acid oxidation yields low volatility organic acids in clouds, Geophys. Res. Lett.,

421   33, 272-288, 2006.

422   Carlton, A. G., Turpin, B. J., Altieri, K. E., Seitzinger, S. P., Mathur, R., Roselle, S. J., and Weber, R. J.: CMAQ

423   Model Performance Enhanced When In-Cloud Secondary Organic Aerosol is Included: Comparisons of Organic

424   Carbon Predictions with Measurements, Environ. Sci. Technol., 42, 8798-8802, 10.1021/es801192n, 2008.

425   Carlton, A. G., Bhave, P. V., Napelenok, S. L., Edney, E. D., Sarwar, G., Pinder, R. W., Pouliot, G. A., and Houyoux,

Atmospheric
Chemistry
and Physics
Discussions

Open Access

426   M.: Model Representation of Secondary Organic Aerosol in CMAQv4.7, Environ. Sci. Technol., 44, 8553-8560,
427   10.1021/es100636q, 2010.

428   Carter, W. P. L.: Implementation of the SAPRC-99 Chemical Mechanism into the Models-3 Framework Report to
429   the US Environmental Protection Agency, Research Triangle Park, NC, 2000.

430   Corrigan, A. L., Hanley, S. W., and De Haan, D. O.: Uptake of glyoxal by organic and inorganic aerosol, Environ.
431   Sci. Technol., 42, 4428-4433, 10.1021/es7032394, 2008.

432   Cotton, W. R., Pielke, R. A., Walko, R. L., Liston, G. E., Tremback, C. J., Jiang, H., McAnelly, R. L., Harrington, J.
433   Y., Nicholls, M. E., Carrio, G. G., and McFadden, J. P.: RAMS 2001: Current status and future directions, Meteorol.
434   Atmos. Phys., 82, 5-29, 10.1007/s00703-001-0584-9, 2003.

435   Curry, L. A., Tsui, W. G., and McNeill, V. F.: Technical note: Updated parameterization of the reactive uptake of
436   glyoxal and methylglyoxal by atmospheric aerosols and cloud droplets, Atmos. Chem. Phys., 18, 9823-9830,
437   10.5194/acp-18-9823-2018, 2018.

438   de Gouw, J. A., Middlebrook, A. M., Warneke, C., Goldan, P. D., Kuster, W. C., Roberts, J. M., Fehsenfeld, F. C.,
439   Worsnop, D. R., Canagaratna, M. R., Pszenny, A. A. P., Keene, W. C., Marchewka, M., Bertman, S. B., and Bates,
440   T. S.: Budget of organic carbon in a polluted atmosphere: Results from the New England Air Quality Study in
441   2002, J. Geophys. Res.-Atmos., 110, 10.1029/2004jd005623, 2005.

442   Emery, C., Tai, E., Yarwood, G.: Enhanced meteorological modeling and performance evaluation for two Texas
443   ozone episodes, In: Prepared for the Texas Natural Resource Conservation Commission, ENVIRON International
444   Corporation, Novato, CA, USA, 2001.

445   Emmons, L. K., Walters, S., Hess, P. G., Lamarque, J. F., Pfister, G. G., Fillmore, D., Granier, C., Guenther, A.,
446   Kinnison, D., Laepple, T., Orlando, J., Tie, X., Tyndall, G., Wiedinmyer, C., Baughcum, S. L., and Kloster, S.:
447   Description and evaluation of the Model for Ozone and Related chemical Tracers, version 4 (MOZART-4), Geosci.
448   Model Dev., 3, 43-67, 2010.

449   Ervens, B., Feingold, G., Frost, G. J., and Kreidenweis, S. M.: A modeling study of aqueous production of
450   dicarboxylic acids: 1. Chemical pathways and speciated organic mass production, J. Geophys. Res.: Atmos., 109,
451   D15205, 10.1029/2003JD004387, 2004.

452   Ervens, B., Turpin, B. J., and Weber, R. J.: Secondary organic aerosol formation in cloud droplets and aqueous
453   particles (aqSOA): a review of laboratory, field and model studies, Atmos. Chem. Phys., 11, 11069-11102,
454   10.5194/acp-11-11069-2011, 2011.

455   Ervens, B., Sorooshian, A., Lim, Y. B., and Turpin, B. J.: Key parameters controlling OH-initiated formation of
456   secondary organic aerosol in the aqueous phase (aqSOA), J. Geophys. Res.-Atmos., 119, 3997-4016,
457   10.1002/2013jd021021, 2014.

458   Feng, T., Bei, N., Huang, R.-J., Cao, J., Zhang, Q., Zhou, W., Tie, X., Liu, S., Zhang, T., Su, X., Lei, W., Molina, L.
459   T., and Li, G.: Summertime ozone formation in Xi'an and surrounding areas, China, Atmos. Chem. Phys., 16,
460   4323-4342, 10.5194/acp-16-4323-2016, 2016.

461   Foley, K. M., Roselle, S. J., Appel, K. W., Bhave, P. V., Pleim, J. E., Otte, T. L., Mathur, R., Sarwar, G., Young, J.
462   O., Gilliam, R. C., Nolte, C. G., Kelly, J. T., Gilliland, A. B., and Bash, J. O.: Incremental testing of the Community
463   Multiscale Air Quality (CMAQ) modeling system version 4.7, Geosci. Model Dev., 3, 205-226, 10.5194/gmd-3-
464   205-2010, 2010.

465   Fu, T.-M., Jacob, D. J., Wittrock, F., Burrows, J. P., Vrekoussis, M., and Henze, D. K.: Global budgets of atmospheric
466   glyoxal and methylglyoxal, and implications for formation of secondary organic aerosols, J. Geophys. Res.-
467   Atmos., 113, 10.1029/2007jd009505, 2008.

468   Fu, T. M., Jacob, D. J., and Heald, C. L.: Aqueous-phase reactive uptake of dicarbonyls as a source of organic aerosol
469   over eastern North America, Atmos. Environ., 43, 1814-1822, 2009.

470   Galloway, M. M., Chhabra, P. S., Chan, A. W. H., Surratt, J. D., Flagan, R. C., Seinfeld, J. H., and Keutsch, F. N.:
471   Glyoxal uptake on ammonium sulphate seed aerosol: reaction products and reversibility of uptake under dark and
472   irradiated conditions, Atmos. Chem. Phys., 9, 3331-3345, 10.5194/acp-9-3331-2009, 2009.

473   Gao, M., Carmichael, G. R., Wang, Y., Saide, P. E., Yu, M., Xin, J., Liu, Z., and Wang, Z.: Modeling study of the
474   2010 regional haze event in the North China Plain, Atmos. Chem. Phys., 16, 1673-1691, 10.5194/acp-16-1673-
475   2016, 2016.

476   Goldstein, A. H., and Galbally, I. E.: Known and unexplored organic constituents in the earth's atmosphere, Environ.
477   Sci. Technol., 41, 1514-1521, 10.1021/es072476p, 2007.

478   Gong, S. L.: A parameterization of sea-salt aerosol source function for sub- and super-micron particles, Global
479   Biogeochem. Cycles, 17, 10.1029/2003gb002079, 2003.

480   Guenther, A. B., Jiang, X., Heald, C. L., Sakulyanontvittaya, T., Duhl, T., Emmons, L. K., and Wang, X.: The Model
481   of Emissions of Gases and Aerosols from Nature version 2.1 (MEGAN2.1): an extended and updated framework
482   for modeling biogenic emissions, Geosci. Model Dev., 5, 1471-1492, 10.5194/gmd-5-1471-2012, 2012.

483   Han, Z., Xie, Z., Wang, G., Zhang, R., and Tao, J.: Modeling organic aerosols over east China using a volatility
484   basis-set approach with aging mechanism in a regional air quality model, Atmos. Environ., 124, Part B, 186-198,
485   http://dx.doi.org/10.1016/j.atmosenv.2015.05.045, 2016.

486   Han, Z. W., Ueda, H., Matsuda, K., Zhang, R. J., Arao, K., Kanai, Y., and Hasome, H.: Model study on particle size
487   segregation and deposition during Asian dust events in March 2002, J. Geophys. Res.-Atmos., 109,
488   10.1029/2004jd004920, 2004.

489   Harrison, R. M., and Yin, J. X.: Particulate matter in the atmosphere: which particle properties are important for its
490   effects on health?, Sci. Total Environ., 249, 85-101, 10.1016/s0048-9697(99)00513-6, 2000.

491   Heald, C. L., Jacob, D. J., Park, R. J., Russell, L. M., Huebert, B. J., Seinfeld, J. H., Liao, H., and Weber, R. J.: A
492   large organic aerosol source in the free troposphere missing from current models, Geophys. Res. Lett., 32,
493   10.1029/2005gl023831, 2005.

494   Hu, J., Wang, P., Ying, Q., Zhang, H., Chen, J., Ge, X., Li, X., Jiang, J., Wang, S., Zhang, J., Zhao, Y., and Zhang,
495   Y.: Modeling biogenic and anthropogenic secondary organic aerosol in China, Atmos. Chem. Phys., 17, 77-92,
496   10.5194/acp-17-77-2017, 2017.

497   Intergovernmental Panel on Climate Change (IPCC): The Physical Science Basis of Climate Change: Changes in
498   Atmospheric Constituents and in Radiative Forcing, Cambridge University Press, New York, pp. 26-27, 2007.

499   Jacob, D. J.: Heterogeneous chemistry and tropospheric ozone, Atmos. Environ., 34, 2131-2159, 10.1016/s1352-
500   2310(99)00462-8, 2000.

501   Juda-Rezler, K., Reizer, M., Huszar, P., Krueger, B. C., Zanis, P., Syrakov, D., Katragkou, E., Trapp, W., Melas, D.,
502   Chervenkov, H., Tegoulias, I., and Halenka, T.: Modelling the effects of climate change on air quality over Central
503   and Eastern Europe: concept, evaluation and projections, Clim. Res., 53, 179-203, 10.3354/cr01072, 2012.

504   Kalberer, M., Paulsen, D., Sax, M., Steinbacher, M., Dommen, J., Prevot, A. S. H., Fisseha, R., Weingartner, E.,
505   Frankevich, V., Zenobi, R., and Baltensperger, U.: Identification of polymers as major components of atmospheric
506   organic aerosols, Science, 303, 1659-1662, 10.1126/science.1092185, 2004.

507   Kanakidou, M., Seinfeld, J. H., Pandis, S. N., Barnes, I., Dentener, F. J., Facchini, M. C., Van Dingenen, R., Ervens,
508   B., Nenes, A., Nielsen, C. J., Swietlicki, E., Putaud, J. P., Balkanski, Y., Fuzzi, S., Horth, J., Moortgat, G. K.,
509   Winterhalter, R., Myhre, C. E. L., Tsigaridis, K., Vignati, E., Stephanou, E. G., and Wilson, J.: Organic aerosol
510   and global climate modelling: a review, Atmos. Chem. Phys., 5, 1053-1123, 2005.

511   Kroll, J. H., Ng, N. L., Murphy, S. M., Flagan, R. C., and Seinfeld, J. H.: Secondary organic aerosol formation from
512   isoprene photooxidation under high-NOx conditions, Geophys. Res. Lett., 32, 10.1029/2005gl023637, 2005.

513   Kroll, J. H., Ng, N. L., Murphy, S. M., Flagan, R. C., and Seinfeld, J. H.: Secondary organic aerosol formation from

Atmospheric
Chemistry
and Physics
Discussions

514   isoprene photooxidation, Environ. Sci. Technol., 40, 1869-1877, 10.1021/es0524301, 2006.

515   Kurokawa, J., Ohara, T., Morikawa, T., Hanayama, S., Janssens-Maenhout, G., Fukui, T., Kawashima, K., and
516   Akimoto, H.: Emissions of air pollutants and greenhouse gases over Asian regions during 2000-2008: Regional
517   Emission inventory in ASia (REAS) version 2, Atmos. Chem. Phys., 13, 11019-11058, 10.5194/acp-13-11019-
518   2013, 2013.

519   Lal, V., Khalizov, A. F., Lin, Y., Galvan, M. D., Connell, B. T., and Zhang, R.: Heterogeneous reactions of epoxides
520   in acidic media, J Phys Chem A, 116, 6078-6090, 10.1021/jp2112704, 2012.

521   Lane, T. E., Donahue, N. M., and Pandis, S. N.: Simulating secondary organic aerosol formation using the volatility
522   basis-set   approach   in   a   chemical   transport   model,   Atmos.   Environ.,   42,   7439-7451,
523   10.1016/j.atmosenv.2008.06.026, 2008.

524   Li, J., Zhang, M., Wu, F., Sun, Y., and Tang, G.: Assessment of the impacts of aromatic VOC emissions and yields
525   of SOA on SOA concentrations with the air quality model RAMS-CMAQ, Atmos. Environ., 158, 105-115,
526   10.1016/j.atmosenv.2017.03.035, 2017a.

527   Li, J., Zhang, M., Tang, G., Wu, F., Alvarado, L. M. A., Vrekoussis, M., Richter, A., and Burrows, J. P.: Investigating
528   missing sources of glyoxal over China using a regional air quality model (RAMS-CMAQ), Journal of
529   Environmental Sciences, 10.1016/j.jes.2018.04.021, 2018.

530   Li, L., Chen, C. H., Huang, C., Huang, H. Y., Zhang, G. F., Wang, Y. J., Wang, H. L., Lou, S. R., Qiao, L. P., Zhou,
531   M., Chen, M. H., Chen, Y. R., Streets, D. G., Fu, J. S., and Jang, C. J.: Process analysis of regional ozone formation
532   over the Yangtze River Delta, China using the Community Multi-scale Air Quality modeling system, Atmos.
533   Chem. Phys., 12, 10971-10987, 10.5194/acp-12-10971-2012, 2012.

534   Li, M., Zhang, Q., Kurokawa, J.-i., Woo, J.-H., He, K., Lu, Z., Ohara, T., Song, Y., Streets, D. G., Carmichael, G. R.,
535   Cheng, Y., Hong, C., Huo, H., Jiang, X., Kang, S., Liu, F., Su, H., and Zheng, B.: MIX: a mosaic Asian
536   anthropogenic emission inventory under the international collaboration framework of the MICS-Asia and HTAP,
537   Atmos. Chem. Phys., 17, 935-963, 10.5194/acp-17-935-2017, 2017b.

538   Li, N., Fu, T.-M., Cao, J., Lee, S., Huang, X.-F., He, L.-Y., Ho, K.-F., Fu, J. S., and Lam, Y.-F.: Sources of secondary
539   organic aerosols in the Pearl River Delta region in fall: Contributions from the aqueous reactive uptake of
540   dicarbonyls, Atmos. Environ., 76, 200-207, 10.1016/j.atmosenv.2012.12.005, 2013.

541   Liggio, J., Li, S. M., and Mclaren, R.: Reactive uptake of glyoxal by particulate matter, Journal of Geophysical
542   Research, 110, 257-266, 2005.

543   Lim, Y. B., and Ziemann, P. J.: Products and mechanism of secondary organic aerosol formation from reactions of
544   n-alkanes with OH radicals in the presence of NOx, Environ. Sci. Technol., 39, 9229-9236, 10.1021/es051447g,
545   2005.

546   Lin, J., An, J., Qu, Y., Chen, Y., Li, Y., Tang, Y., Wang, F., and Xiang, W.: Local and distant source contributions to
547   secondary organic aerosol in the Beijing urban area in summer, Atmos. Environ., 124, Part B, 176-185,
548   http://dx.doi.org/10.1016/j.atmosenv.2015.08.098, 2016.

549   Lin, Y.-H., Zhang, H., Pye, H. O. T., Zhang, Z., Marth, W. J., Park, S., Arashiro, M., Cui, T., Budisulistiorini, H.,
550   Sexton, K. G., Vizuete, W., Xie, Y., Luecken, D. J., Piletic, I. R., Edney, E. O., Bartolotti, L. J., Gold, A., and
551   Surratt, J. D.: Epoxide as a precursor to secondary organic aerosol formation from isoprene photooxidation in the
552   presence of nitrogen oxides, Proceedings of the National Academy of Sciences of the United States of America,
553   110, 6718-6723, 10.1073/pnas.1221150110, 2013.

554   Liu, Z., Wang, Y., Vrekoussis, M., Richter, A., Wittrock, F., Burrows, J. P., Shao, M., Chang, C.-C., Liu, S.-C., Wang,
555   H., and Chen, C.: Exploring the missing source of glyoxal (CHOCHO) over China, Geophys. Res. Lett., 39,
556   10.1029/2012gl051645, 2012.

557   Loeffler, K. W., Koehler, C. A., Paul, N. M., and De Haan, D. O.: Oligomer formation in evaporating aqueous glyoxal

Atmospheric
Chemistry
and Physics
Discussions

558   and methyl glyoxal solutions, Environ. Sci. Technol., 40, 6318-6323, 10.1021/es060810w, 2006.

559   Morris, R. E., McNally, D. E., Tesche, T. W., Tonnesen, G., Boylan, J. W., and Brewer, P.: Preliminary evaluation of

560   the community multiscale air, quality model for 2002 over the southeastern United States, Journal of the Air &

561   Waste Management Association, 55, 1694-1708, 10.1080/10473289.2005.10464765, 2005.

562   Morris, R. E., Koo, B., Guenther, A., Yarwood, G., McNally, D., Tesche, T. W., Tonnesen, G., Boylan, J., and Brewer,

563   P.: Model sensitivity evaluation for organic carbon using two multi-pollutant air quality models that simulate

564   regional   haze   in   the   southeastern   United   States,   Atmos.   Environ.,   40,   4960-4972,

565   10.1016/j.atmosenv.2005.09.088, 2006.

566   Murphy, B. N., and Pandis, S. N.: Simulating the Formation of Semivolatile Primary and Secondary Organic Aerosol

567   in a Regional Chemical Transport Model, Environ. Sci. Technol., 43, 4722-4728, 10.1021/es803168a, 2009.

568   Murphy, D. M., Cziczo, D. J., Froyd, K. D., Hudson, P. K., Matthew, B. M., Middlebrook, A. M., Peltier, R. E.,

569   Sullivan, A., Thomson, D. S., and Weber, R. J.: Single-particle mass spectrometry of tropospheric aerosol particles,

570   J. Geophys. Res.: Atmos., 111, n/a-n/a, 10.1029/2006jd007340, 2006.

571   Myriokefalitakis, S., Vrekoussis, M., Tsigaridis, K., Wittrock, F., Richter, A., Bruehl, C., Volkamer, R., Burrows, J.

572   P., and Kanakidou, M.: The influence of natural and anthropogenic secondary sources on the glyoxal global

573   distribution, Atmos. Chem. Phys., 8, 4965-4981, 2008.

574   Ng, N. L., Kroll, J. H., Chan, A. W. H., Chhabra, P. S., Flagan, R. C., and Seinfeld, J. H.: Secondary organic aerosol

575   formation from m-xylene, toluene, and benzene, Atmos. Chem. Phys., 7, 3909-3922, 2007.

576   Poschl, U.: Atmospheric aerosols: Composition, transformation, climate and health effects, Angewandte Chemie-

577   International Edition, 44, 7520-7540, 10.1002/anie.200501122, 2005.

578   Randerson, J.T., van der Werf, G.R., Giglio, L., Collatz, G.J., Kasibhatla, P.S.: Global fire emissions database,

579   version 4 (GFEDv4), Data set available on-line (http://daac.ornl.gov/) from Oak Ridge National Laboratory

580   Distributed Active Archive Center, Oak Ridge, Tennessee, USA, https://doi.org/10.3334/ ORNLDAAC/1293,

581   2015.

582   Roberts, M. C., Andreae, M. O., Zhou, J. C., and Artaxo, P.: Cloud condensation nuclei in the Amazon Basin:

583   "Marine" conditions over a continent?, Geophys. Res. Lett., 28, 2807-2810, 2001.

584   Shrivastava, M. K., Lane, T. E., Donahue, N. M., Pandis, S. N., and Robinson, A. L.: Effects of gas particle

585   partitioning and aging of primary emissions on urban and regional organic aerosol concentrations, J. Geophys.

586   Res.-Atmos., 113, 10.1029/2007jd009735, 2008.

587   Sun, J., Wu, F., Hu, B., Tang, G., Zhang, J., and Wang, Y.: VOC characteristics, emissions and contributions to SOA

588   formation during hazy episodes, Atmos. Environ., 141, 560-570, 10.1016/j.atmosenv.2016.06.060, 2016.

589   Surratt, J. D., Lewandowski, M., Offenberg, J. H., Jaoui, M., Kleindienst, T. E., Edney, E. O., and Seinfeld, J. H.:

590   Effect of acidity on secondary organic aerosol formation from isoprene, Environ. Sci. Technol., 41, 5363-5369,

591   10.1021/es0704176, 2007.

592   Volkamer, R., Jimenez, J. L., San Martini, F., Dzepina, K., Zhang, Q., Salcedo, D., Molina, L. T., Worsnop, D. R.,

593   and Molina, M. J.: Secondary organic aerosol formation from anthropogenic air pollution: Rapid and higher than

594   expected, Geophys. Res. Lett., 33, 10.1029/2006gl026899, 2006.

595   Wang, F., An, J., Li, Y., Tang, Y., Lin, J., Qu, Y., Chen, Y., Zhang, B., and Zhai, J.: Impacts of uncertainty in AVOC

596   emissions on the summer ROx budget and ozone production rate in the three most rapidly-developing economic

597   growth regions of China, Advances in Atmospheric Sciences, 31, 1331-1342, 10.1007/s00376-014-3251-z, 2014.

598   Warneck, P.: In-cloud chemistry opens pathway to the formation of oxalic acid in the marine atmosphere, Atmos.

599   Environ., 37, 2423-2427, 10.1016/s1352-2310(03)00136-5, 2003.

600   Willmott,   C.   J.:   ON   THE   VALIDATION   OF   MODELS,   Physical   Geography,   2,   184-194,

601   10.1080/02723646.1981.10642213, 1981.

602   Wu, F., Yu, Y., Sun, J., Zhang, J., Wang, J., Tang, G., and Wang, Y.: Characteristics, source apportionment and
603   reactivity of ambient volatile organic compounds at Dinghu Mountain in Guangdong Province, China, Sci. Total
604   Environ., 548, 347-359, http://dx.doi.org/10.1016/j.scitotenv.2015.11.069, 2016.
605   Xu, W., Han, T., Du, W., Wang, Q., Chen, C., Zhao, J., Zhang, Y., Li, J., Fu, P., Wang, Z., Worsnop, D. R., and Sun,
606   Y.: Effects of Aqueous-Phase and Photochemical Processing on Secondary Organic Aerosol Formation and
607   Evolution in Beijing, China, Environ. Sci. Technol., 51, 762-770, 10.1021/acs.est.6b04498, 2017.
608   Xu, W. Q., Sun, Y. L., Chen, C., Du, W., Han, T. T., Wang, Q. Q., Fu, P. Q., Wang, Z. F., Zhao, X. J., Zhou, L. B., Ji,
609   D. S., Wang, P. C., and Worsnop, D. R.: Aerosol composition, oxidation properties, and sources in Beijing: results
610   from the 2014 Asia-Pacific Economic Cooperation summit study, Atmos. Chem. Phys., 15, 13681-13698,
611   10.5194/acp-15-13681-2015, 2015.
612   Ying, Q., Li, J., and Kota, S. H.: Significant Contributions of Isoprene to Summertime Secondary Organic Aerosol
613   in Eastern United States, Environ. Sci. Technol., 49, 7834-7842, 10.1021/acs.est.5b02514, 2015.
614   Yu, S., Mathur, R., Schere, K., Kang, D., Pleim, J., Young, J., Tong, D., Pouliot, G., McKeen, S. A., and Rao, S. T.:
615   Evaluation of real-time PM2.5 forecasts and process analysis for PM2.5 formation over the eastern United States
616   using the Eta-CMAQ forecast model during the 2004 ICARTT study, J. Geophys. Res.-Atmos., 113,
617   10.1029/2007jd009226, 2008.
618   Zhang, H., and Ying, Q.: Secondary organic aerosol formation and source apportionment in Southeast Texas, Atmos.
619   Environ., 45, 3217-3227, 10.1016/j.atmosenv.2011.03.046, 2011.
620   Zhang, H., Li, J., Ying, Q., Yu, J. Z., Wu, D., Cheng, Y., He, K., and Jiang, J.: Source apportionment of PM2.5 nitrate
621   and sulfate in China using a source-oriented chemical transport model, Atmos. Environ., 62, 228-242,
622   https://doi.org/10.1016/j.atmosenv.2012.08.014, 2012.
623   Zhang, Q., Jimenez, J. L., Canagaratna, M. R., Allan, J. D., Coe, H., Ulbrich, I., Alfarra, M. R., Takami, A.,
624   Middlebrook, A. M., Sun, Y. L., Dzepina, K., Dunlea, E., Docherty, K., DeCarlo, P. F., Salcedo, D., Onasch, T.,
625   Jayne, J. T., Miyoshi, T., Shimono, A., Hatakeyama, S., Takegawa, N., Kondo, Y., Schneider, J., Drewnick, F.,
626   Borrmann, S., Weimer, S., Demerjian, K., Williams, P., Bower, K., Bahreini, R., Cottrell, L., Griffin, R. J.,
627   Rautiainen, J., Sun, J. Y., Zhang, Y. M., and Worsnop, D. R.: Ubiquity and dominance of oxygenated species in
628   organic aerosols in anthropogenically-influenced Northern Hemisphere midlatitudes, Geophys. Res. Lett., 34,
629   10.1029/2007gl029979, 2007.

630
631
632
633
634
635
636
637
638
639
640

641 Table 1. Statistics for the meteorological variables and PM$_{2.5}$ between the simulated and observed data during the

642 two episodes.

Table 1-1

Variables	Episode	N	C_{mod}	C_{obs}	MB	RMSE	R	IOA
Temperature	1	10770	23.76	24.59	−0.83	2.58	0.86	0.91
(ºC)	2	8391	12.68	13.36	−0.68	3.13	0.92	0.95
Relative humidity	1	10770	69.42	67.90	1.52	13.68	0.83	0.91
(%)	2	8389	62.81	62.86	−0.05	14.73	0.77	0.88
Wind speed	1	10770	1.78	2.18	−0.40	1.64	0.35	0.61
(m/s)	2	8391	2.05	2.27	−0.22	1.75	0.50	0.69

Table 1-2

Variables	Episode	N	C_{mod}	C_{obs}	FB (%)	FE (%)	R	IOA
PM$_{2.5}$	1	8091	64.04	47.90	13.35	64.61	0.50	0.64
(μg/m^3)	2	7649	86.25	61.67	36.00	62.27	0.56	0.70

Table 1-3

Variables	Episode	N	P$_{22.5°}$ (%)	P$_{45°}$ (%)
Wind direction	1	10770	32.12	54.52
(°)	2	8391	34.01	57.41

643 N is the total number of samples; C_{mod} and C_{obs} are the average value of modeled and observed results, respectively;

644 MB and FB are the mean and fractional bias, respectively; RMSE and FE are the root-mean-square and fractional

645 error, respectively; IOA is the index of agreement; R is the correlation coefficient between the observed and simulated

646 results; P$_{22.5°}$ and P$_{45°}$ represent the proportions of compared results that the absolute biases between the simulated

647 and measured wind directions are within 22.5° and 45°, respectively.

648

649 Table 2. Performance statistics of the modeled and observed SOA concentrations (μg/m^3).

Case	Episode	N	C_{model}	C_{obs}	MB	RMSE	R	IOA
0	1	822	2.21	12.69	−10.48	13.48	0.21	0.46
	2	737	1.05	17.69	−16.64	23.52	0.83	0.45
1	1	822	3.78	12.69	−8.91	12.16	0.30	0.48
	2	737	1.31	17.69	−16.38	23.10	0.80	0.46
2	1	822	7.33	12.69	−5.36	10.10	0.27	0.50
	2	737	3.02	17.69	−14.67	20.79	0.80	0.51

650

Atmospheric
Chemistry
and Physics
Discussions

Open Access

EGU
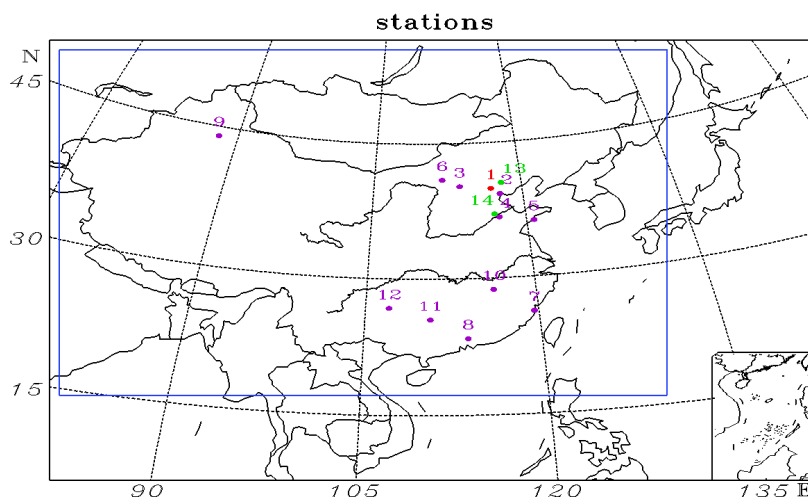
651

652 Fig. 1. Geographical locations of the measurement stations in the model domain. 1: Beijing; 2: Tianjin; 3: Datong;

653 4: Jinan; 5: Qingdao; 6: Hohhot; 7: Fuzhou; 8: Guangzhou; 9: Urumqi; 10: Nanchang; 11: Guilin; 12: Guiyang; 13:

654 Xinglong; 14: Yucheng. The different colors denote which variables are compared at each station: purple:

655 meteorological parameters; green: concentrations of aromatics; red: both meteorological parameters and aromatic

656 compound concentrations.

657
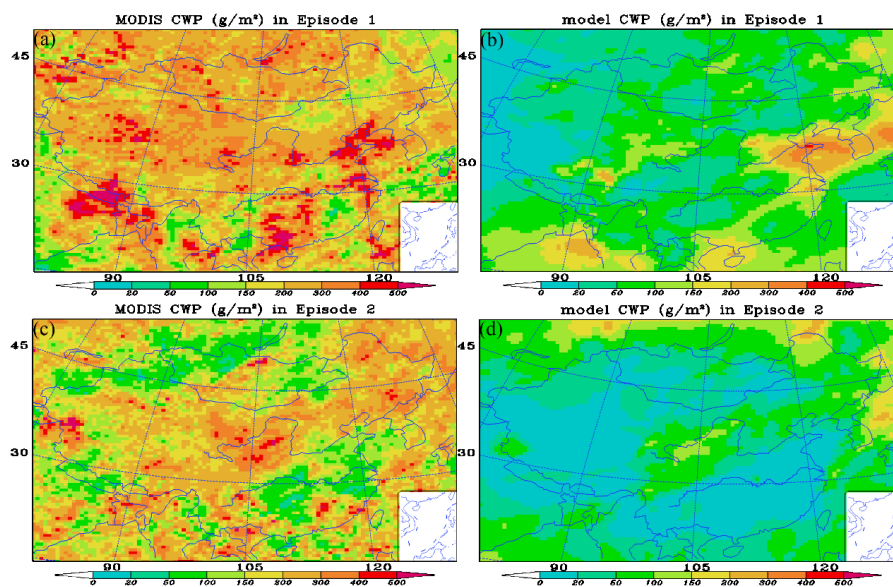
658

659 Fig. 2. Observed and simulated distributions of the mean cloud water path (CWP) during the two episodes (left-hand

660 panels: MODIS observation; right-hand panels: results of simulations).

Atmospheric
Chemistry
and Physics
Discussions
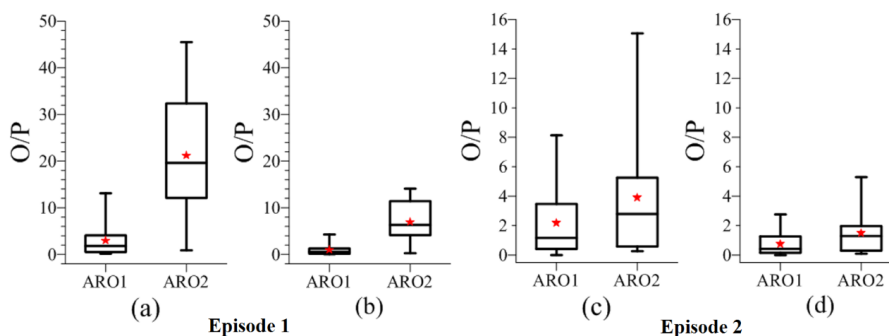
Fig. 3. Box-whisker plot of the observed to predicted (O/P) ratios of aromatic compounds during the two analyzed episodes at three sites (Beijing, Xinglong and Yucheng). (a, c): Original emissions of aromatic compounds; and (b, d): a three-fold increase in the emissions of aromatic compounds. The red stars show the mean O/P ratios.
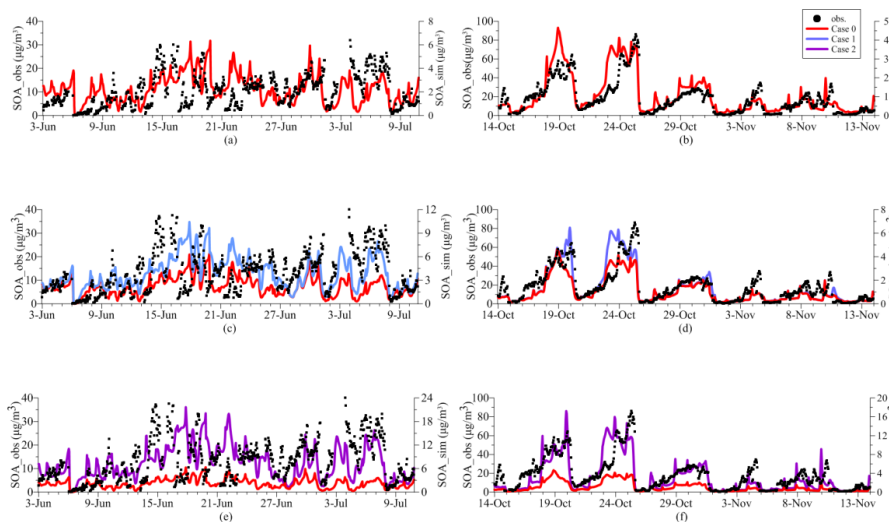
Fig. 4. Hourly concentrations of the observed and simulated near-surface SOA concentrations in the two analyzed episodes. (a, b) Case 0 is base run; (c, d) case 1 is run with the incorporation of the aqueous irreversible uptake of dicarbonyls; and (e, f) case 2 is run with the glyoxal underestimation taken into consideration based on case 1.

Atmospheric
Chemistry
and Physics
Discussions

670
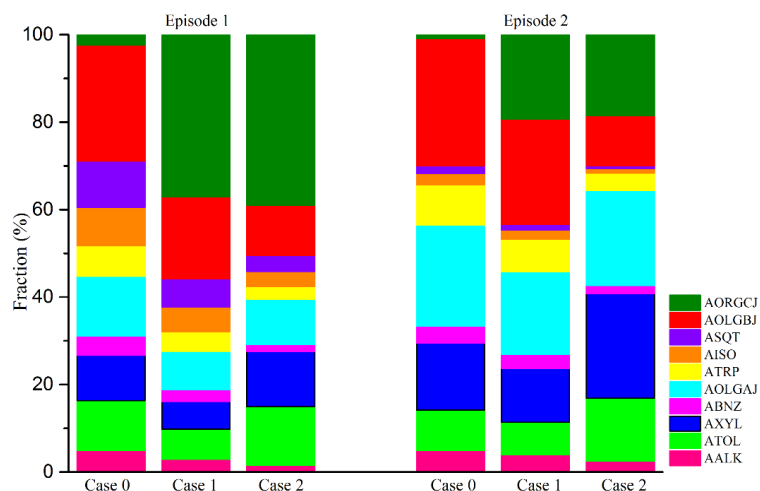
Fig. 5. Mean contributions from different sources of SOAs in the three sensitivity case studies during the two analyzed episodes. The compositions represent the SOA formed from long-chain alkanes (AALK), high-yield aromatic compounds (ATOL), low-yield aromatic compounds (AXYL), benzene (ABNZ), monoterpenes (ATRP), isoprene (AISO) and dicarbonyls (AORGCJ), as well as aged anthropogenic (AOLGAJ) and biogenic SOA (AOLGBJ). Case 0 is the base run; case 1 is run with the incorporation of the aqueous irreversible uptake of dicarbonyls; and case 2 is based on case 1, but taking into consideration the underestimation of glyoxal.

677

678
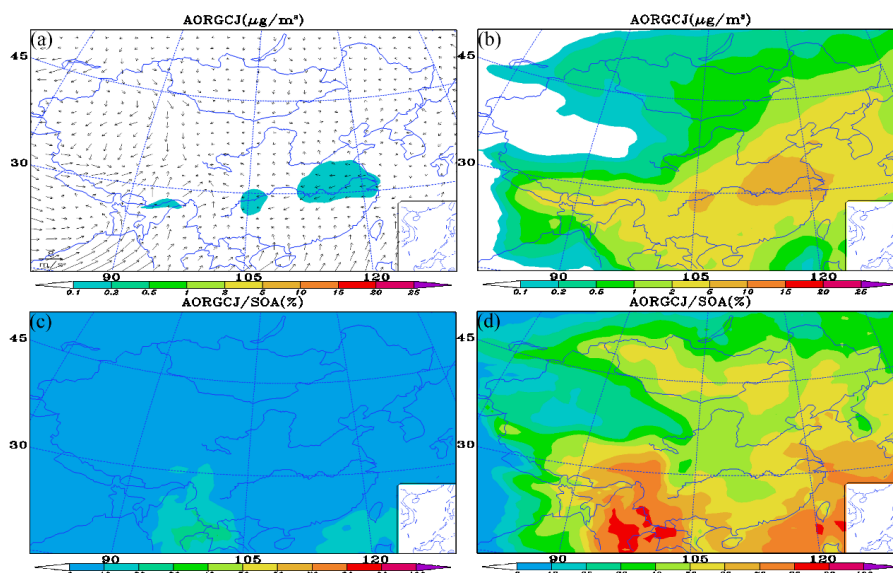
Fig. 6. Modeled distributions of the mean (a) wind field with AORGCJ in case 0, (b) AORGCJ in case 2, (c)

680   AORGCJ/SOA in case 0, (d) AORGCJ/SOA in case 2, over the regions during episode 1. Case 0 is the base run;

681   case 2 is run taking into consideration the incorporation of the aqueous irreversible uptake of dicarbonyls and the

682   underestimation of glyoxal.